HHS Public Access

Author manuscript

Biomaterials. Author manuscript; available in PMC 2016 September 01.

Published in final edited form as:

Biomaterials. 2015 September ; 62: 24–34. doi:10.1016/j.biomaterials.2015.05.021.

Decreasing matrix modulus of PEG hydrogels induces a vascular phenotype in human cord blood stem cells

Shruthi Mahadevaiah[1,2], **Karyn G. Robinson**[1], **Prathamesh M. Kharkar**[3], **Kristi L. Kiick**[3], and **Robert E. Akins**[1,*]

[1]Nemours – Alfred I. duPont Hospital for Children, Department of Biomedical Research, 1600 Rockland Road, Wilmington, DE 19803

[2]Nemours – Alfred I. duPont Hospital for Children, Critical Care Department, 1600 Rockland Road, Wilmington, DE 19803

[3]Department of Materials Science and Engineering, University of Delaware, 201 Du Pont Hall, Newark, DE 19716

Abstract

Adult and congenital cardiovascular diseases are significant health problems that are often managed using surgery. Bypass grafting is a principal therapy, but grafts fail at high rates due to hyperplasia, fibrosis, and atherosclerosis. Biocompatible, cellularized materials that attenuate these complications and encourage healthy microvascularization could reduce graft failure, but an improved understanding of biomaterial effects on human stem cells is needed to reach clinical utility. Our group investigates stem-cell-loaded biomaterials for placement along the adventitia of at-risk vessels and grafts. Here, the effects of substrate modulus on human CD34+ stem cells from umbilical cord blood were evaluated. Cells were isolated by immunomagnetic separation and encapsulated in 3, 4, and 6 weight% PEG hydrogels containing 0.032% gelatin and 0.0044% fibronectin. Gels reached moduli of 0.34, 4.5, and 9.1 kPa. Cell viability approached 100%. Cell morphologies appeared similar across gels, but proliferation was significantly lower in 6 wt% gels. Expression profiling using stem cell signaling arrays indicated enhanced self-renewal and differentiation into vascular endothelium among cells in the lower weight percent gels. Thus, modulus was associated with cell proliferation and function. Gels with moduli in the low kilopascal range may be useful in stimulating cell engraftment and microvascularization of graft adventitia.

*For correspondence: Robert E. Akins, PhD, Director, Center for Pediatric Clinical Research and Development, Nemours – Alfred I. duPont Hospital for Children, 1600 Rockland road, Wilmington, DE 19803, Robert.Akins@nemours.org, Phone: (302) 651 – 6811, FAX: (302) 651 – 6897.

1. Introduction

Cardiovascular diseases are substantial health problems across all age groups accounting for ~17% of health care expenditures [1]. Congenital heart defects are the most common, most costly, and most deadly type of birth defect in children, and coronary and peripheral artery diseases are leading causes of morbidity, mortality, and health-related expenses in adults. Vascular reconstructive surgery is a main treatment for these diseases, and a variety of grafts including autologous tissue, preserved allografts, synthetic conduits, and tissue engineered grafts are being used in attempts to optimize surgical results. Unfortunately, 20 to 50% of vascular grafts fail [2, 3] due to intimal hyperplasia, fibrosis, thrombosis, and atherosclerosis. There is a need for methods to increase the survival of vascular grafts, and regenerative strategies, including advanced biomaterials and tissue engineered vessels, are in development [4, 5]. An easy to use, biocompatible, cellularized biomaterial that could be placed along the abluminal surface of grafted vessels to redirect maladaptive responses, re-establish healthy microvasculature, and increase graft healing and survival would have significant appeal. Our group is working to develop stem cell-loaded PEG hydrogels for this purpose.

Stem cells can play major roles in biomaterials-based regenerative therapies. They can be readily prepared from host tissues, have significant self-renewal potential, and differentiate into specific cell lineages depending on their microenvironment. They can provide a cell source to support functional regeneration, serve as cytokine factories, and recent data indicate they may even function as immune sentinels [6]. Stem cells are being used to generate and replace a variety of tissue types. For example, embryonic stem cells have been transplanted into rats with spinal cord injury for remyelination and restoration of locomotion [7]. Mesenchymal stem cells have been used to create a tissue engineered human trachea that has functioned for the last 5 years [8] and have shown promise for the treatment of myocardial infarction [9]. Recently, tissue resident stem cells from human retinal pigment epithelium were grown on a polyester matrix and transplanted into rats with age-related macular degeneration with success [10]. Of particular relevance, CD34+ stem cells have been associated with enhanced healing, secretion of anti-inflammatory molecules, and revascularization of injured tissue [11–14]. These attributes recommend CD34+ cells as strong candidates for cellularized biomaterials for placement along vascular grafts, and CD34+ cells are assessed in the present work.

Since matrix and substrate conditions can strongly impact cell phenotype [15, 16], there is a need to develop materials that can mimic matrices and provide predictable control over stem cell fate while allowing facile delivery of the cells to appropriate sites. In particular, studies have shown that matrix stiffness affects cell adhesion, migration, proliferation, and differentiation [17–19]. PEG-based hydrogels are excellent candidates that provide tunable mechanical and chemical properties and allow three-dimensional cell culture mimicking in-vivo cellular environments [20]. PEG gels are relatively inert to cell adhesion but can be combined with cell adhesion proteins like fibronectin, collagen, laminin, or adhesion oligopeptides [21]. Hydrogels are already being used as implantable devices for drug delivery, tissue engineering, and cell based drug production [22–25].

Our previous work with heparin-containing PEG hydrogels of various moduli and human vascular endothelial, smooth muscle, and aortic adventitial fibroblastic cells showed differential adhesion, proliferation, and gene expression was associated with the modulus of the hydrogel in a cell type-dependent manner [26, 27]. Thus, the choice of material and its stiffness to be used for biomedical applications are critical design characteristics for controlling the fate of cells. Although blood vessels have elastic moduli in the range of 100s of kPa to MPas [28–30], the outer adventitial layer contributes little to this stiffness and is characterized by relatively loose structure [29, 31]. The outer adventitia has a suspected modulus similar to stroma or soft tissue in the <10kPa range. Accordingly, in the current study, the effect of PEG hydrogels in this (<10kPa) modulus range on encapsulated CD34+ stem cells' morphology, proliferation, and gene expression in three dimensional cell culture was investigated to help guide the development of therapies to improve the survival of vascular grafts.

2. Materials and Methods

2.1 Stem cell isolation from cord blood

Deidentified samples of cord blood were obtained from Community Blood Services (Allendale, NJ). Cells were isolated using reagents and protocols from Miltenyi Biotec (Bergisch Gladbach, Germany) unless otherwise noted. Anticoagulated cord blood samples were diluted 1:4 with cold autoMACS Rinsing Solution and mononuclear cells were isolated using Ficoll-Paque Premium (GE Healthcare, Pittsburgh, PA) at a specific gravity of 1.078 g/cc. Density centrifugation was performed at 400 x g for 35 minutes. The mononuclear cell layer was collected and transferred to a separate tube. Cells were washed three times with autoMACS Rinsing Solution. The final cell pellet was resuspended in 500μl of MACS BSA buffer and passed through a 30μm nylon mesh pre-separation filter. Magnetic beads coated with a monoclonal antibody specific for human CD34 were used to separate CD34+ cells. First, 100μl of FcR blocking reagent and 100μl of CD34 microbeads were added to every 300μl cells and incubated for 30 minutes at 4°C. Cells were washed once by centrifugation and resuspended in 500μl MACS BSA buffer. CD34+ cells were then isolated using magnetic cell separation. Cells were applied to an LS column containing ferromagnetic spheres in the presence of a strong magnetic field and rinsed with 3ml MACS BSA buffer three times; the magnetic beads and bound cells were retained in the column. The column was removed from the magnetic field, and the labeled cells were collected by flushing the column. Target cells were further purified over a second column following the same procedure. Cells were centrifuged at 300 x g for 10 minutes and the cell pellet was resuspended in StemSpan H3000 medium with CC100 cytokine cocktail (STEMCELL Technologies, Vancouver, British Columbia), 100 U/mL penicillin, and 100 μg/mL streptomycin (Mediatech, Herndon, VA) and cultured at 37°C.

2.2 Flow Cytometry

Cells were enumerated using a hemocytometer and resuspended in 1x MACS BSA solution to a final concentration of 10^7 cells/ml. 100μl of this cell suspension (10^6cells) was transferred to each of four sterile Eppendorf tubes. 10μl of phycoerythrin-conjugated CD34 antibody (CD34-PE; Miltenyi Biotec) was added to two tubes and incubated for 10 minutes

at 4°C. Cells were washed with 1ml D-PBS, centrifuged at 300 x g for 10 minutes, and the supernatant was aspirated. Cells were then fixed with 500μl of 2% PFA (Electron Microscopy Sciences, Hatfield, PA) for 30 minutes. Cells were permeablized by adding 5μl of 0.1% Triton-X 100 (Sigma) to all tubes for 15 minutes. Cells were washed and resuspended in 1ml Dulbecco's PBS (D-PBS), pH 7.4. To label nuclei, 3μl of DRAQ5 (Thermo Fisher Scientific, Rockford, IL) was added to two tubes to yield a final concentration of 15 μM After 40 minutes of incubation, the four vials of cells (unstained, CD34-PE stained, DRAQ5 stained, and double stained) were characterized by flow cytometry using an Accuri C6 Flow Cytometer (BD Biosciences).

2.3 Stem cell encapsulation in PEG hydrogel

Four- arm maleimide-functionalized poly(ethylene glycol) (PEG, f = 4, M_n 10,000 g/mol, JenKem Technology USA, Chicago, IL) and four-arm thiol-funtionalized PEG (f = 4, M_n 10,000 g/mol, JenKem Technology USA) were used to form gel networks to encapsulate human CD34+ stem cells. Fibronectin and gelatin were incorporated into the hydrogels via reaction with the maleimide-functionalized PEG to provide cell-adhesive materials. First, human fibronectin (FN; BD Biosciences) and type A porcine gelatin (Fisher Scientific; 275 Bloom) were mixed with PEG-$(maleimide)_4$ in 10 mM citrate buffer, pH 4.5, to achieve final concentrations of 0.044 mg/ml FN and 0.32 mg/ml gelatin. These concentrations were determined empirically using the FN and gelatin components were mixed with the PEG-maleimide to allow their attachment to the PEG prior to hydrogel formation. PEG-$(SH)_4$ was dissolved in StemSpan H300 medium and both PEG solutions were separately sterilized by passing the solutions through 0.2 μm polyethersulfone (PES) filters (EMD Millipore, Billerica, MA). CD34+ stem cells suspended in StemSpan H3000 medium were first suspended in the PEG-$(SH)_4$ solution then mixed with the PEG-$(maleimide)_4$ solution to form 100μl gels in 35 mm glass bottom culture dishes (MatTek Corp, Ashland, MA). Three different moduli of hydrogels (comprising 3, 4 and 6 wt% PEG) were prepared by altering the concentration of PEG. Hydrogels of a concentration of 3wt% comprised 2mM PEG-$(maleimide)_4$ and 1mM PEG-$(SH)_4$; 4wt% hydrogels comprised 2mM PEG-$(maleimide)_4$ and 2mM PEG-$(SH)_4$; and 6wt% hydrogels comprised 3mM PEG-$(maleimide)_4$ and 3mM PEG-$(SH)_4$. After gelation, medium was flooded over each gel to a volume of 3 mL. The hydrogel cultures were placed in 37°C incubators in HEPA-filtered air supplemented with 5% CO_2.

2.4 Rheological characterization of hydrogels

The mechanical properties of the hydrogels were studied using bulk oscillatory rheology (ARG-2, TA instruments, New Castle, DE, USA). Briefly, hydrogel precursor solutions with a 2:1 maleimide:thiol stoichiometric ratio for 3% hydrogels and a 1:1 ratio for 4% and 6% hydrogels along with fibronectin and type A gelatin were added to a cylindrical mold (diameter = 4.6 mm, thickness = 1.8 mm) and allowed to gel for two hours at 37°C. Subsequently, the hydrogels were incubated with StemSpan H3000 medium for 24 hours at 4°C, and the hydrogels were carefully loaded onto the geometry of an oscillatory rheometer to measure their elastic storage moduli The equilibrium swollen moduli of hydrogels were determined using a 20 mm stainless steel parallelplate geometry under the linear viscoelastic regime (2% strain and 2 rad/s frequency)..

2.5 Microscopy, viability assay

CD34+ cells were encapsulated in 100μL of hydrogel at a density of 2×10^4 cells/gel. Photomicrography was carried out using a Leica Fluovert inverted microscope with Hoffman modulation contrast at 10x magnification. Cells were imaged using a Hamamatsu ORCA camera (Hamamatsu Photonics, Japan) and Image-Pro Plus software (version 6.3; Media Cybernetics, Rockville, MD). Viability of the encapsulated stem cells was assessed using SYTO13, which is a membrane-permeant, nuclear stain, and propidium iodide (PI), which labels nuclei of necrotic cells. The gels were washed once with D-PBS, and PI (500 ng/ml; Miltenyi) and SYTO13 (50 μM; Life Technologies) in D-PBS were added and incubated for 15 minutes at room temperature. The samples were then rinsed, fixed for 1 hour with 2% paraformaldehyde, rinsed again, mounted with a cover slip, and viewed using an Olympus BX-60 fluorescence microscope with an Evolution QEi,12-bit digital camera (Media Cybernetics) with Image-Pro Plus software (version 6.3; Media Cybernetics).

2.6 RNA preparation

Triplicate hydrogels of each weight percent were seeded with 1×10^6 cells per 100 μL volume, and cultured. At culture termination, gels were transferred to 1.5ml RNase-free tubes and immediately frozen in dry ice/methanol. The hydrogels were pulverized using a motorized Teflon pestle, and 700μl of TRI Reagent (Molecular Research Center) was added to dissolve the samples, denature proteins, and stabilize RNA. Samples were incubated for 5 minutes at room temperature to permit the complete dissociation of nucleoprotein complexes followed by 10 minutes at 60°C. Subsequently, 140μl of chloroform was thoroughly mixed into each sample at room temperature for 15 minutes before centrifuging at 4°C for 15 minutes at 12,000 x g. The upper phase, which contained the RNA, was collected and 350μl of isopropanol was added. Samples were held at room temperature for 10 minutes then centrifuged at 12,000 x g for 8 minutes at 4°C. The RNA pellets were washed once with 75% ethanol, and samples from the same modulus gel were pooled (n=3) in 87.5μl of DEPC- treated water (Fisher). DNase treatment and RNA clean-up were performed using an RNeasy Mini Kit (Qiagen, Valencia, CA) according to the manufacturer's instructions. The RNA concentration was measured immediately using an ND-1000 NanoDrop spectrophotometer (NanoDrop Technologies, Wilmington, DE) and stored at −80°C.

2.7 qPCR assay

Gene expression was analyzed using RT^2 Profiler PCR arrays (Qiagen). cDNA synthesis and Real Time PCR were performed according to protocols from the manufacturer. Briefly, 100ng of RNA was reverse transcribed using an RT^2 First Strand Kit, and the resulting cDNA was mixed with RT^2 SYBR Green/ROX qPCR Master Mix and loaded into a Stem Cell Signaling 384-well PCR Array containing optimized primers; 84 test genes plus 5 housekeeper genes and controls were analyzed per sample. Real-time PCR detection was performed on an ABI7900HT with a thermal cycling profile of 1 cycle at 95°C for 10 min, followed by 40 cycles of 95°C for 15s and 60°C for 1 min. Results were analyzed using Qiagen's PCR Array Data Analysis Web Portal. Cells grown without hydrogel (i.e. over tissue culture polystyrene) for seven days were used as controls (n=5 TCPS samples with one sample chosen as the calibrator), and ACTB, B2M, GAPDH, HPRT1, and RPLP0 were

considered housekeeping genes. Genes for which no Ct values were less than 30 were excluded. Any hydrogel sample with an expression change greater than 2-fold from the TCPS calibrator or more than 1.96 standard deviations from the TCPS mean were considered significant. Heat maps were created using The Institute for Genome Research (TIGR) MultiExperiment Viewer (TMeV).

2.8 Antibody staining for von Willebrand Factor and morphology assessment

PEG hydrogels were cryosectioned by the Histochemistry and Tissue Processing Core Laboratory of Nemours-A.I. duPont Hospital for Children using a protocol adapted from Ruan et al. [32]. Briefly, PEG hydrogels were removed from culture medium and fixed with 4% paraformaldehyde for 30 minutes, rinsed, and then infiltrated with Tissu-Tek® Optimal Cutting Temperature embedding medium (OCT; Sakura-Finetek, Torrance, CA) overnight at 4°C. Samples were rinsed with fresh OCT and placed in a chilled well of the Precision Cryoembedding System (Pathology Innovations, Wyckoff, NJ) within a −21°C cryostat (Leica CM 3050S). The well was filled with additional OCT and topped with a cryostat chuck. Samples were stored at −80°C and 10 μm cryosections were obtained from the frozen blocks using a cryostat (Leica CM 3050S) at −21°C. Section s were permeabilized with 0.1% Triton X-100 (Sigma) for 15 min, blocked with 3% bovine serum albumin in D-PBS (Sigma) for 30 min, and stained with a rabbit antibody against vWF (1:200 in D-PBS to yield a final concentration of 40 μg/mL; Abcam, Cambridge, MA) followed by an Alexa Fluor-conjugated secondary antibody (Life Technologies) and bisbenzamide (Hoechst 33258 in D-PBS). Samples were digitally imaged on an Olympus BX-60 fluorescence microscope equipped with an Evolution QEi monochrome 12-bit digital camera (Media Cybernetics) controlled by Image Pro Plus software (version 6.3; Media Cybernetics). Cell morphology was analyzed by staining samples with Alexa Fluor 488-conjugated phalloidin and Hoechst 33258, imaging at 40x, and measuring cell area and aspect ratio (n>25 cells for each modulus) using Image Pro Plus.

3. Results

3.1 Hydrogel composition and characterization

Among various natural and synthetic polymeric materials available for hydrogel formation, PEG-based hydrogels have emerged as promising candidates for various bioengineering applications due to excellent biocompatibility, high hydrophilicity, and lack of inherent protein binding sites. [33] In the present study, maleimide and thiol end-functionalized PEG macromers were used to generate stable crosslinks via a Michael-type addition reaction (Figure 1). Michael-type additions are a class of click reactions that are highly efficient and occur under mild physiological conditions without any byproduct. [34, 35] Fibronectin and gelatin were covalently incorporated within the hydrogel network to provide cell attachment sites and were included to allow cells to interact with the hydrogels. Fibronectin and collagen are both found in arterial adventitia (see [29] for review) and were used in combination to provide a biomimetic environment. The concentrations of these components were determined using a cell adhesion and growth assay based on the ability of human fibroblast cells (aortic adventitial fibroblasts) to adhere, spread, and proliferate on the surface of 6wt% PEG hydrogels (data not shown). Diffusion of the fibronectin and gelatin

components was limited by reacting their free cysteine residues with PEG-$(maleimide)_4$. Subsequently, PEG-$(SH)_4$ was combined with the PEG-$(maleimide)_4$ solution at room temperature to form highly elastic hydrogels. The concentration of PEG polymer was varied to permit assessment of the response of encapsulated cells to various material moduli.

Gelation kinetics and final storage moduli were measured using dynamic time sweep assays in the linear viscoelastic regime. Representative storage moduli evaluated during hydrogel formation are shown in Supplementary Figure 1. A crossover point between the storage and loss moduli, which is an estimate of gel point, was not observed due to rapid gelation before the first data point was acquired (data not shown), indicating that highly elastic networks were formed in < 60 seconds (which was the minimum time required to acquire the first data point after mixing the precursor solutions). The nucleophilicity of the thiolate species can be reduced by employing acidic buffer conditions, which significantly affects the Michael-type addition reaction kinetics. [36–38] Hence, the hydrogels were prepared under slightly acidic pH to limit the rate of gelation sufficiently to permit the production of uniform and homogeneous hydrogels. The storage moduli of swollen hydrogel discs (diameter = 4.6 mm, thickness = 1.8 mm) were also measured via oscillatory rheometry in the linear viscoelastic regime after preparing the hydrogels. After their initial gelation, hydrogel discs were swollen for 24 hours at 4°C in StemSpan H3000 medium. The equilibrium storage moduli for the 3, 4, and 6 weight % hydrogels after this incubation with medium were found to be 0.34, 4.5, and 9.1 kPa as shown in Figure 2. As per the theory of rubber elasticity, the material stiffness is correlated with the network crosslinking density [39] with an increase in the concentration of polymer, the crosslinking density increases, leading to an increased modulus. Overall, these results indicate that the stable hydrogels containing appropriate biochemical cues and having tailorable stiffness can be reliably produced to study cell response when cells are encapsulated in the 3-D matrices with tailorable mechanical properties.

3.2 Flow cytometric analysis of isolated cells

The preparation of CD34-positive stem cells from human cord blood by immunomagnetic separation was validated by flow cytometry. After isolation and culture in StemSpan H300 medium, the purity of isolated cells was characterized using an Accuri C6 Flow Cytometer. Unstained cells were used to establish gating parameters for the cytometer, and DRAQ5, which stains cell nuclei, was used to verify cytometer settings. Anti-CD34-PE was used to enumerate positive cells (Supplementary Figure 2). Based on single channel analysis, 93.4% of cells were positive for CD34. The immunomagnetic separation approach was used to prepare cells for subsequent culture experiments. These results validate the purification scheme and were consistent with previous studies with isolated stem cells. [40]

3.3 Morphology and viability of encapsulated stem cells

In previous studies, PEG based hydrogels of different moduli were used to culture different types of cells (NIH3T3, AoAFs, HUVECs and T/G HA) on gel surfaces. [27] Different cell types showed varied attachment, proliferation, and gene expression profiles when cultured on the PEG-based hydrogels depending on the hydrogel modulus. As seen in Figure 3A, there were no significant differences in area or aspect ratio (p=0.10 and 0.18, respectively,

by Kruskal-Wallis Test; see Supplementary Figure 3) of the encapsulated stem cells on day 7 as indicated using Hoffman modulation contrast microscopy. Cells remained similar and generally round in shape in the 3, 4 and 6 wt% hydrogels with aspect ratios ranging from 1.28 to 1.45. To assess the viability of the encapsulated cells, they were stained with propidium iodide and SYTO13. As seen in Figure 3B, there was fluorescence only for SYTO13 and none for propidium iodide in the encapsulated stem cells in 3, 4 and 6 wt% hydrogels on culture day 7. Similar results were seen immediately after the initiation of culture on day one. These observations indicate that cells encapsulated in all three moduli of hydrogel were viable on days one and 7 with virtually no dead cells present.

3.4 Cell proliferation

Proliferation of the encapsulated stem cells was assessed by directly counting cells within 5 randomly selected gel subvolumes in each sample. Subvolumes were defined as the column of gel delimited by the field of view of the 10x objective employed. The average cell count of stem cells in hydrogels of each modulus was 110.8±7.6, 100.4±5.0 and 71.0±6.8 (n=5 distinct gel subvolumes for each) for the 3, 4 and 6wt% hydrogels, respectively. As seen in Figure 4, the proliferation of encapsulated stem cells was significantly higher in the 3 wt% and 4 wt% hydrogels versus the 6 wt% hydrogel ($p= 0.005$ and $p= 0.008$ respectively by ANOVA with Tukey's HSD posthoc test). There were no statistically significant differences in the proliferation of encapsulated stem cells between 3 and 4 wt% hydrogels.

3.5 Gene expression analysis

RT^2 Profiler PCR arrays against genes associated with human stem cell signaling were used to assess differences in gene expression. Samples were collected after 7 days from 3, 4, and 6 wt% hydrogel cultures and comparator cell cultures grown over TCPS. Ct values for 84 target genes plus 5 housekeeping controls were analyzed using RT^2 Profiler PCR Array Data Analysis software (version 3.5). Targets with all Ct values greater than 30 were considered to be "not present." Those that exhibited a statistically significant difference in expression level relative to at least one other group were included in subsequent analyses; 38 of the 84 target genes were included.

Gene expression levels in the hydrogel cultures were calibrated against levels in cells grown using standard TCPS. Any hydrogel sample with an expression change greater than 2-fold from the TCPS calibrator or more than 1.96 standard deviations from the TCPS mean (n=5 TCPS samples) were considered significant. As shown in Table 1, fold differences ranged from ~10-fold increases to ~8-fold decreases. The 38 genes represented all six of the pathways interrogated (i.e., pluripotency maintenance, FGF, Hedgehog, Notch, TGF-β, and Wnt signaling), but genes in TGF-β pathways were statistically over-represented ($p<0.05$ by Fisher Exact Test) accounting for 23 hits. Among the genes most highly affected by hydrogel culture, 10 exhibited differences more than ~5 fold: ACVR2B, FGFR1, LTBP2, NOTCH3, and SMAD7 were all significantly increased, especially in the 3 and/or 4 wt% gels; ACVRL1, CTNNB1, ENG, SUFU, TGFBRAP1 were all significantly decreased, especially in the 6 wt% gels. Interestingly, several of these genes have specific roles in endothelial cell biology and blood vessel formation. Among the up-regulated genes, ACVR2B and LTBP2 are both involved in canonical TGF-β signaling, FGFR1 is a well-

established mediator of vascular endothelial cell function and angiogenesis [41], NOTCH3 has been linked with cell-contact mediated vascular smooth muscle cell differentiation [42], and SMAD7 is a critical modulator of TGF-β signaling in endothelial cells [43] and associated with adventitial cell function [44]. All five of the genes with significantly reduced expression are linked to endothelial cell function and/or angiogenesis. Thus, a principal response to hydrogel culture seems to have been alteration in gene expression associated with vascularization with the 6 wt% gels generally resulting in inhibition while the lower wt % gels resulted in activation of critical pathways.

To visualize and categorize expression patterns across hydrogel moduli, the data were converted to z-scores relative to the average expression for each gene considered separately. Hierarchical clustering analysis carried out using The Institute for Genome Research's Multiple Experiment Viewer (TMeV) software allowed genes with similar expression patterns to be clustered together. Six clusters were identified for the 38 target genes as indicated in Table 1 and Figure 5. A heat map generated from the z-score values shows the relationship among the genes (Figure 5). Heat map colors represent the relative mRNA expression above or below the average of the three hydrogel samples with blue indicating lower than average expression and red indicating higher. Graphical representations of the z-score plot for each gene in the clusters are shown in Supplementary Figure 4.

3.6 Antibody staining from encapsulated cells

Since the results of the mRNA analysis indicated an elevation in endothelial cell gene expression in the lower modulus gels, we sought to evaluate the endothelial cell content of encapsulated cells using immunostaining for von Willebrand Factor (vWF). vWF is a well-characterized marker of endothelial cells, and as can be seen in Figure 6, vWF-positive cells appeared in groups within the PEG hydrogels. There appeared to be more vWF positive in larger groupings in the low weight percent gels (3 and 4 wt%) than in the higher weight percent gels. These observations are consistent with the molecular data described above and support the interpretation that decreased modulus promoted endothelial cell differentiation.

4. Discussion

The results presented here indicate that culture within PEG-based materials with bulk moduli in the low to sub kilopascal range can dramatically influence the phenotype of clinically-relevant human stem cells. Cells grown within the lower weight percent gels exhibited gene expression profiles indicative of an angiogenic/vasculogenic phenotype suggesting that relatively soft gels might foster therapeutic angiogenesis if placed along grafted blood vessels. Therapeutic angiogenesis is a complex process that requires production of specific factors [45] and significant recruitment of cells [31] that may not happen routinely in standard vein-to-artery grafts. The development of materials that can support the delivery of cells primed to support graft revascularization would provide both of these conditions and would represent a significant advance. Our results indicate that PEG-based hydrogels may be excellent candidates for this purpose. The PEG hydrogels employed in this study are easy to prepare, can be tuned by the clinician to desired composition and modulus, and can be readily delivered in tight spaces and along complex anatomical surfaces.

Interestingly, any effects of gel modulus would be intimately related to the availability of cell binding ligands within the 3D matrix and other gel properties. Polymer weight percent, stiffness of the branches, hydrostatic pressure, and substrate fluidity are all determinants of ligand availability and cell behavior and all linked to each other. [46–49] It is, therefore, difficult to ascribe the results seen in the present work solely to modulus. In particular, the availability of the fibronectin and gelatin cell-binding ligands may vary across gels with a relative decrease in availability in the 6 wt% gels. It should be noted, however, that in the present study, the concentrations of cell binding components were selected based on cell binding and spreading assays carried out in 2D culture and, thus, at least partially optimized. Also, although the morphometric measures of cell cross-sectional area and aspect ratio in the CD34+ cells did not vary significantly across the gels (see Supplementary Figure 3), aspect ratios tended to be greater in the higher weight percent gels; whereas, decreasing ligand density might be expected to lead to more spherical cells. These observations suggest potentially complex interactions among the biophysical characteristics of polymer weight percent, stiffness, hydrostatic pressure, and fluidity that, in aggregate, have significant effects on human stem cell phenotype.

Our study employed populations of CD34+ cells from de-identified human cord blood. Cord blood represents a potentially important source of therapeutic stem cells, but CD34+ cells can also be prepared from other tissues, including fat. Importantly, the cells used here were prepared using a clinically-accessible immunomagnetic separation strategy (Supplementary Figure 1) and, therefore, represent a clinically feasible stem cell population. Many studies have shown that stem cell behaviors are affected by their microenvironment, including the stiffness of the growth matrix, [18, 19] the growth medium, [31] and the chemokines present or the chemistry of the material used. [50, 51] In the present study, these characteristics were controlled at the outset of culture, but subsequent changes in cytokine release as cells responded to their initial culture environment or in the overall density of cells in the matrix, which varied during culture since proliferation rates varied, may have elicited secondary effects on the cells. The cascade of potential events that may lead to CD34+ stem cell differentiation into vascular tissues combined with the complexity of the interacting physicochemical properties of the hydrogel system make it difficult to define specific mechanistic pathways; nonetheless, gel weight percent and substrate modulus were directly associated with phenotypic differences in the human CD34+ cells used here.

Previous work by our group with human vascular endothelial, aortic smooth muscle, and aortic adventitial fibroblastic cells supports the notion that varying hydrogel polymer weight percent and modulus within narrow ranges can have a dramatic impact on cell proliferation and phenotype in a cell-type dependent manner. [26, 27] Here, we encapsulated human stem cells prepared from cord blood to study the effect of culture in PEG hydrogels of different weight percent polymer without exogenous growth factors or chemokines. Oscillatory rheology showed that the bulk modulus of the gel formulations was reproducibly controlled (Figure 2), and encapsulated cells exhibited excellent viability (Figure 3) indicating that the gel formulations were highly supportive of human stem cells. Interestingly, we found that proliferation was significantly higher in the softer gels and decreased as the modulus was increased (Figure 4). These results are consistent with the previously reported effects of materials with modulus in the kilopascal range on neural stem cells from rats, which also

exhibit decreased proliferation with increasing gel stiffness. [18] Rodent neural stem cells have also been shown to switch phenotype in softer versus stiffer gels. [18, 19] Studies looking at substrates that were orders of magnitude stiffer than the ones employed here indicated that TG2α E14 mouse embryonic stem cell differentiation to mesodermal lineages occurred at lower moduli compared to osteogenic differentiation at higher moduli. [52] It should be noted, however, that the TCPS control cultures carried out for the present work did not involve the attachment of the CD34+ cells to the surface, which is orders of magnitude stiffer than the hydrogels. In fact, the control cells were suspended, and the ~10^8 Pa modulus of the TCPS was not expected to influence the cells. Thus, our results are consistent with previous work but focus on the design of materials to influence the phenotype of clinically-relevant human stem cells to a desirable vascular phenotype.

We performed stem cell signaling array analysis on the RNA extracted from encapsulated CD34+ stem cells to assess 84 genes involved in signal transduction pathways needed for stem cell maintenance and differentiation. Out of these 84 genes, 38 genes had statistically significant differences in expression relative to cells grown in standard culture. The most highly affected genes were FGFR1, LTBP2, and NOTCH3, which were significantly up-regulated in all hydrogels tested. These genes were all expressed at low levels in the control, suspension culture samples in our study. In previous studies using cord-blood derived CD34+ cells and with data published in the Gene Expression Omnibus [53], the probesets for all three of these genes had signals associated with expression levels close to zero. Thus, the relatively large fold increases seen in the expression of these three genes in hydrogels may simply result from expression being turned-on by hydrogel culture. In each of these three cases, the genes are associated with blood vessel formation: For example, FGFR1 has been associated with the balance among modulatory cytokines affecting vascular endothelial cell function; [54] LTBP2 has been associated with arterial elasticity; [55] NOTCH3 has been associated with blood vessel integrity. [56]

The application of a non-biased hierarchical clustering algorithm revealed 6 different patterns of expression in these 38 genes across hydrogel formulations (Figure 5). A significant number of genes were down-regulated as the PEG polymer increased to 6wt% (Clusters 4 and 5; accounting for 18 of the 38 genes identified). Several genes had complex patterns in which expression in the 4wt% gels was significantly higher (Clusters 2 and 3; accounting for 13 genes) or lower (Cluster 6; accounting for 4 genes) than the 3 and 6 wt% gels. ACVR1 was the only gene identified with a trend of increasing expression in the 3, to 4, to 6 wt% gels. This ACVR1 result suggests that aspects of TGF-β signaling may be elevated by increasing modulus; however, the situation is complex since fully 23 of the 38 genes flagged in our assays were associated with TGF-β signaling (Table 1) and TGF-β super-family pathway members are represented in all 6 clusters.

Members of the TGF-β super-family are involved in the regulation of proliferation, differentiation, and survival of many types of cells [57] and play key roles in vasculogenesis and angiogenesis. [58] Receptors in this family comprise two types: type I receptors or activin-like receptors (e.g., ACVR1) and type II receptors, which are generally referred to by their ligand (e.g., BMPR1A). There are more than 33 ligands in the TGF-β pathways, including the bone morphogenetic proteins (BMPs), growth and differentiation factors

(GDFs), activins, and nodal. [58] Receptor activation by these ligands results in SMAD-mediated signaling to affect gene expression. In our study, genes representing both types of receptors were differentially expressed across gel types as were several related signaling intermediates (i.e., SMADs) belonging to TGF-β pathways. These results indicate a fundamental alteration in TGF-β-related cell function associated with the weight percent of the gels. Interestingly, several Wnt signaling pathway genes were also strikingly affected with five Wnt signal mediators altered. Wnt is involved in stem cell pluripotency and self-renewal, and the data suggest increased Wnt signaling in the low wt% gels.

Of note, most of the genes in clusters 3, 4, and 5, which all exhibit the lowest level of expression in the 6 wt% gels, belonged to the TGF-β superfamily, The genes in cluster 5, which showed steadily decreasing expression as weight percent increased, are of particular interest. ACVRL1, also known as ALK-1, is an endothelial-specific TGF-β type 1 receptor, which upon activation induces phosphorylation of SMAD1/5/8; these activated SMADs form complexes that translocate into the nucleus to activate or repress angiogenic genes. [59] Regulation of vascular formation by ACVRL1 is only partially understood, but it plays important roles, and blocking it during postnatal development in mice has been shown to cause arteriovenous malformation. [60] ENG (Endoglin, or CD105) is a co-receptor in the TGF-β family; it is expressed highly in vascular endothelium and is important for the development of the vascular system. It has been shown that expression of ENG in human mesenchymal stem cells increases cardiac regenerative potential in mice with myocardial infarction [61] and that even though vasculogenesis can occur with ENG-deficient embryonic stem cells, ENG is required for the formation of tubular structures from stem cell derived endothelial cells. [62] FGFR1, fibroblast growth factor receptor 1, stimulates endothelial cells and vascularization in response to activation by several different FGFs. Recent studies have shown that FGFR1 signaling also stimulates proliferation of human stem cells and may help to maintain their multi-lineage potential. [63] LTBP3 encodes a protein that may be involved in the assembly, secretion, and targeting of TGF-β1 to sites where it is stored or activated and may also have a structural role in the extracellular matrix. NCSTN, a subunit of the gamma-secretase complex, catalyzes the intramembrane cleavage of integral membrane proteins such as Notch receptors and amyloid precursor protein and acts as regulator of angiogenesis through several mechanisms. [64] The SMAD4 gene encodes a protein that acts both as a transcription factor and as a tumor suppressor. SMAD4 is suspected to support self-renewal and pluripotency maintenance, and a recent study showed that it is needed to stabilize the stem cell pluripotent state. [65] When SMAD4 was overexpressed in human hematopoietic stem/progenitor cells, it led to impaired reconstitution and negatively regulated self-renewal of these cells in vivo. [66] TGFBRAP1 is a receptor that associates with inactive heteromeric TGF-β and activin receptor complexes that may recruit SMAD4 to facilitate its interaction with other SMADs. Overall, the expression profiles suggest that the lower wt% gels supported self-renewal and a shift in phenotype toward vascular structure formation. Immunofluorescence localization of vascular endothelial cells (Figure 6) supports this interpretation as a significantly larger number of vWF-positive cells were seen in the softer gels. With specific analysis of the genes in cluster 5, it seems clear that the CD34+ stem cells are up-regulating genes associated with the formation of vascular endothelium, tubular structures, and extracellular

matrix that are all needed for vascular graft healing but also have genes involved in self-renewal of these stem cells.

5. Conclusions

This study demonstrates that PEG hydrogels with tunable moduli in the kilopascal range are biocompatible with human stem cells and capable of significantly altering cell behavior. Three dimensional encapsulation of clinically-relevant populations of CD34+ cells significantly affected proliferation and differentiation. Cell proliferation increased with decreasing modulus, and culture in the lower modulus PEG hydrogels was associated with an up-regulation in markers for differentiation to vascular endothelium and associated structures and with stem cell self-renewal. Thus, the modulus of hydrogels used to support encapsulated stem cells is a critical design characteristic for injectable, cellularized biomaterials, and the range of effective gel moduli may be in the kilopascal range with relatively small changes in bulk rheologic characteristics resulting in substantial effects. PEG gels spiked with matrix proteins and having moduli in the low kilopascal range may prove useful in vascular graft repair.

Supplementary Material

Refer to Web version on PubMed Central for supplementary material.

Acknowledgments

The authors thank the Histochemistry and Tissue Processing Core Laboratory of Nemours-A.I. duPont Hospital for Children for assistance with sample preparation. Chris McGann and Eric Levenson are thanked for their helpful discussion and suggestions. This publication was made possible by support from the National Institute of General Medical Sciences IDeA Program (P20 GM103446 to REA and P20 RR017716 to KLK), by funds from the Nemours Foundation (to REA), the University of Delaware Research Foundation (to KLK), and by support from the National Heart Lung and Blood Institute (R01 HL108110 to REA).

References

1. Trogdon JG, Finkelstein EA, Nwaise IA, Tangka FK, Orenstein D. The economic burden of chronic cardiovascular disease for major insurers. Health promotion practice. 2007; 8:234–42. [PubMed: 17606951]
2. Fitzgibbon GM, Kafka HP, Leach AJ, Keon WJ, Hooper GD, Burton JR. Coronary bypass graft fate and patient outcome: angiographic follow-up of 5,065 grafts related to survival and reoperation in 1,388 patients during 25 years. Journal of the American College of Cardiology. 1996; 28:616–26. [PubMed: 8772748]
3. Goldman S, Zadina K, Moritz T, Ovitt T, Sethi G, Copeland JG, et al. Long-term patency of saphenous vein and left internal mammary artery grafts after coronary artery bypass surgery: results from a Department of Veterans Affairs Cooperative Study. Journal of the American College of Cardiology. 2004; 44:2149–56. [PubMed: 15582312]
4. Shinoka T, Breuer C. Tissue-engineered blood vessels in pediatric cardiac surgery. The Yale journal of biology and medicine. 2008; 81:161–6. [PubMed: 19099046]
5. Zhang WJ, Liu W, Cui L, Cao Y. Tissue engineering of blood vessel. Journal of cellular and molecular medicine. 2007; 11:945–57. [PubMed: 17979876]
6. Zhao JL, Ma C, O'Connell RM, Mehta A, DiLoreto R, Heath JR, et al. Conversion of danger signals into cytokine signals by hematopoietic stem and progenitor cells for regulation of stress-induced hematopoiesis. Cell stem cell. 2014; 14:445–59. [PubMed: 24561084]

7. Keirstead HS, Nistor G, Bernal G, Totoiu M, Cloutier F, Sharp K, et al. Human embryonic stem cell-derived oligodendrocyte progenitor cell transplants remyelinate and restore locomotion after spinal cord injury. The Journal of neuroscience : the official journal of the Society for Neuroscience. 2005; 25:4694–705. [PubMed: 15888645]
8. Gonfiotti A, Jaus MO, Barale D, Baiguera S, Comin C, Lavorini F, et al. The first tissue-engineered airway transplantation: 5-year follow-up results. Lancet. 2014; 383:238–44. [PubMed: 24161821]
9. Telukuntla KS, Suncion VY, Schulman IH, Hare JM. The advancing field of cell-based therapy: insights and lessons from clinical trials. Journal of the American Heart Association. 2013; 2:e000338. [PubMed: 24113326]
10. Stanzel BV, Liu Z, Somboonthanakij S, Wongsawad W, Brinken R, Eter N, et al. Human RPE Stem Cells Grown into Polarized RPE Monolayers on a Polyester Matrix Are Maintained after Grafting into Rabbit Subretinal Space. Stem cell reports. 2014; 2:64–77. [PubMed: 24511471]
11. Kanji S, Das M, Aggarwal R, Lu J, Joseph M, Pompili VJ, et al. Nanofiber-expanded human umbilical cord blood-derived CD34(+) cell therapy accelerates cutaneous wound closure in NOD/SCID mice. Journal of cellular and molecular medicine. 2014; 18:685–97. [PubMed: 24455991]
12. Kanji S, Das M, Aggarwal R, Lu J, Joseph M, Basu S, et al. Nanofiber-expanded human umbilical cord blood-derived CD34+ cell therapy accelerates murine cutaneous wound closure by attenuating pro-inflammatory factors and secreting IL-10. Stem cell research. 2014; 12:275–88. [PubMed: 24321844]
13. Huang X, Sun K, Zhao YD, Vogel SM, Song Y, Mahmud N, et al. Human CD34+ progenitor cells freshly isolated from umbilical cord blood attenuate inflammatory lung injury following LPS challenge. PloS one. 2014; 9:e88814. [PubMed: 24558433]
14. Subrammaniyan R, Amalorpavanathan J, Shankar R, Rajkumar M, Baskar S, Manjunath SR, et al. Application of autologous bone marrow mononuclear cells in six patients with advanced chronic critical limb ischemia as a result of diabetes: our experience. Cytotherapy. 2011; 13:993–9. [PubMed: 21671823]
15. Hinz B. Formation and function of the myofibroblast during tissue repair. The Journal of investigative dermatology. 2007; 127:526–37. [PubMed: 17299435]
16. Hoeben A, Landuyt B, Highley MS, Wildiers H, Van Oosterom AT, De Bruijn EA. Vascular endothelial growth factor and angiogenesis. Pharmacological reviews. 2004; 56:549–80. [PubMed: 15602010]
17. Peyton SR, Kim PD, Ghajar CM, Seliktar D, Putnam AJ. The effects of matrix stiffness and RhoA on the phenotypic plasticity of smooth muscle cells in a 3-D biosynthetic hydrogel system. Biomaterials. 2008; 29:2597–607. [PubMed: 18342366]
18. Banerjee A, Arha M, Choudhary S, Ashton RS, Bhatia SR, Schaffer DV, et al. The influence of hydrogel modulus on the proliferation and differentiation of encapsulated neural stem cells. Biomaterials. 2009; 30:4695–9. [PubMed: 19539367]
19. Saha K, Keung AJ, Irwin EF, Li Y, Little L, Schaffer DV, et al. Substrate modulus directs neural stem cell behavior. Biophysical journal. 2008; 95:4426–38. [PubMed: 18658232]
20. DeVolder R, Kong HJ. Hydrogels for in vivo-like three-dimensional cellular studies. Wiley interdisciplinary reviews. Systems biology and medicine. 2012; 4:351–65. [PubMed: 22615143]
21. Peyton SR, Raub CB, Keschrumrus VP, Putnam AJ. The use of poly(ethylene glycol) hydrogels to investigate the impact of ECM chemistry and mechanics on smooth muscle cells. Biomaterials. 2006; 27:4881–93. [PubMed: 16762407]
22. Bhattarai N, Gunn J, Zhang M. Chitosan-based hydrogels for controlled, localized drug delivery. Advanced drug delivery reviews. 2010; 62:83–99. [PubMed: 19799949]
23. Jiang Y, Chen J, Deng C, Suuronen EJ, Zhong Z. Click hydrogels, microgels and nanogels: emerging platforms for drug delivery and tissue engineering. Biomaterials. 2014; 35:4969–85. [PubMed: 24674460]
24. Schmidt JJ, Rowley J, Kong HJ. Hydrogels used for cell-based drug delivery. Journal of biomedical materials research Part A. 2008; 87:1113–22. [PubMed: 18837425]
25. DeVolder RJ, Kong HJ. Three dimensionally flocculated proangiogenic microgels for neovascularization. Biomaterials. 2010; 31:6494–501. [PubMed: 20538334]

26. Robinson KG, Nie T, Baldwin AD, Yang EC, Kiick KL, Akins RE Jr. Differential effects of substrate modulus on human vascular endothelial, smooth muscle, and fibroblastic cells. Journal of biomedical materials research Part A. 2012; 100:1356–67. [PubMed: 22374788]
27. Nie T, Akins RE Jr, Kiick KL. Production of heparin-containing hydrogels for modulating cell responses. Acta biomaterialia. 2009; 5:865–75. [PubMed: 19167277]
28. Cabrera Fischer EI, Bia D, Camus JM, Zocalo Y, de Forteza E, Armentano RL. Adventitia-dependent mechanical properties of brachiocephalic ovine arteries in in vivo and in vitro studies. Acta Physiol (Oxf). 2006; 188:103–11. [PubMed: 16948797]
29. Wagenseil JE, Mecham RP. Vascular extracellular matrix and arterial mechanics. Physiol Rev. 2009; 89:957–89. [PubMed: 19584318]
30. Lu X, Yang J, Zhao JB, Gregersen H, Kassab GS. Shear modulus of porcine coronary artery: contributions of media and adventitia. Am J Physiol Heart Circ Physiol. 2003; 285:H1966–75. [PubMed: 14561679]
31. Stenmark KR, Yeager ME, El Kasmi KC, Nozik-Grayck E, Gerasimovskaya EV, Li M, et al. The adventitia: essential regulator of vascular wall structure and function. Annual review of physiology. 2013; 75:23–47.
32. Ruan JL, Tulloch NL, Muskheli V, Genova EE, Mariner PD, Anseth KS, et al. An improved cryosection method for polyethylene glycol hydrogels used in tissue engineering. Tissue engineering Part C, Methods. 2013; 19:794–801. [PubMed: 23448137]
33. Kharkar PM, Kiick KL, Kloxin AM. Designing degradable hydrogels for orthogonal control of cell microenvironments. Chemical Society reviews. 2013; 42:7335–72. [PubMed: 23609001]
34. Phelps EA, Enemchukwu NO, Fiore VF, Sy JC, Murthy N, Sulchek TA, et al. Maleimide cross-linked bioactive PEG hydrogel exhibits improved reaction kinetics and cross-linking for cell encapsulation and in situ delivery. Advanced materials. 2012; 24:64–70. 2. [PubMed: 22174081]
35. Mather BD, Viswanathan K, Miller KM, Long TE. Michael addition reactions in macromolecular design for emerging technologies. Prog Polym Sci. 2006; 31:487–531.
36. Schelte P, Boeckler C, Frisch B, Schuber F. Differential reactivity of maleimide and bromoacetyl functions with thiols: application to the preparation of liposomal diepitope constructs. Bioconjugate chemistry. 2000; 11:118–23. [PubMed: 10639094]
37. Baldwin AD, Kiick KL. Reversible maleimide-thiol adducts yield glutathione-sensitive poly(ethylene glycol)-heparin hydrogels. Polymer chemistry. 2013; 4:133–43. [PubMed: 23766781]
38. Kharkar PM, Kloxin AM, Kiick KL. Dually degradable click hydrogels for controlled degradation and protein release. Journal of Materials Chemistry B. 2014
39. Treloar, LRG. The physics of rubber elasticity. 3. Oxford; New York: Clarendon Press ; Oxford University Press; 2005.
40. Kekarainen T, Mannelin S, Laine J, Jaatinen T. Optimization of immunomagnetic separation for cord blood-derived hematopoietic stem cells. BMC cell biology. 2006; 7:30. [PubMed: 16882340]
41. Presta M, Dell'Era P, Mitola S, Moroni E, Ronca R, Rusnati M. Fibroblast growth factor/fibroblast growth factor receptor system in angiogenesis. Cytokine & growth factor reviews. 2005; 16:159–78. [PubMed: 15863032]
42. Xia Y, Bhattacharyya A, Roszell EE, Sandig M, Mequanint K. The role of endothelial cell-bound Jagged1 in Notch3-induced human coronary artery smooth muscle cell differentiation. Biomaterials. 2012; 33:2462–72. [PubMed: 22204979]
43. Valdimarsdottir G, Goumans MJ, Itoh F, Itoh S, Heldin CH, ten Dijke P. Smad7 and protein phosphatase 1alpha are critical determinants in the duration of TGF-beta/ALK1 signaling in endothelial cells. BMC cell biology. 2006; 7:16. [PubMed: 16571110]
44. Mallawaarachchi CM, Weissberg PL, Siow RC. Smad7 gene transfer attenuates adventitial cell migration and vascular remodeling after balloon injury. Arteriosclerosis, thrombosis, and vascular biology. 2005; 25:1383–7.
45. Brudno Y, Ennett-Shepard AB, Chen RR, Aizenberg M, Mooney DJ. Enhancing microvascular formation and vessel maturation through temporal control over multiple pro-angiogenic and pro-maturation factors. Biomaterials. 2013; 34:9201–9. [PubMed: 23972477]

46. Kuriyama S, Theveneau E, Benedetto A, Parsons M, Tanaka M, Charras G, et al. In vivo collective cell migration requires an LPAR2-dependent increase in tissue fluidity. J Cell Biol. 2014; 206:113–27. [PubMed: 25002680]
47. Butcher DT, Alliston T, Weaver VM. A tense situation: forcing tumour progression. Nat Rev Cancer. 2009; 9:108–22. [PubMed: 19165226]
48. Chaudhuri O, Koshy ST, Branco da Cunha C, Shin JW, Verbeke CS, Allison KH, et al. Extracellular matrix stiffness and composition jointly regulate the induction of malignant phenotypes in mammary epithelium. Nat Mater. 2014; 13:970–8. [PubMed: 24930031]
49. Engler A, Bacakova L, Newman C, Hategan A, Griffin M, Discher D. Substrate compliance versus ligand density in cell on gel responses. Biophysical journal. 2004; 86:617–28. [PubMed: 14695306]
50. Grimaldi A, Bianchi C, Greco G, Tettamanti G, Noonan DM, Valvassori R, et al. In vivo isolation and characterization of stem cells with diverse phenotypes using growth factor impregnated biomatrices. PloS one. 2008; 3:e1910. [PubMed: 18382683]
51. Liu G, Li Y, Sun J, Zhou H, Zhang W, Cui L, et al. In vitro and in vivo evaluation of osteogenesis of human umbilical cord blood-derived mesenchymal stem cells on partially demineralized bone matrix. Tissue engineering Part A. 2010; 16:971–82. [PubMed: 19839720]
52. Evans ND, Minelli C, Gentleman E, LaPointe V, Patankar SN, Kallivretaki M, et al. Substrate stiffness affects early differentiation events in embryonic stem cells. European cells & materials. 2009; 18:1–13. discussion -4. [PubMed: 19768669]
53. Oswald J, Steudel C, Salchert K, Joergensen B, Thiede C, Ehninger G, et al. Gene-expression profiling of CD34+ hematopoietic cells expanded in a collagen I matrix. Stem cells. 2006; 24:494–500. [PubMed: 16166251]
54. Magnusson PU, Dimberg A, Mellberg S, Lukinius A, Claesson-Welsh L. FGFR-1 regulates angiogenesis through cytokines interleukin-4 and pleiotrophin. Blood. 2007; 110:4214–22. [PubMed: 17875810]
55. Shipley JM, Mecham RP, Maus E, Bonadio J, Rosenbloom J, McCarthy RT, et al. Developmental expression of latent transforming growth factor beta binding protein 2 and its requirement early in mouse development. Mol Cell Biol. 2000; 20:4879–87. [PubMed: 10848613]
56. Henshall TL, Keller A, He L, Johansson BR, Wallgard E, Raschperger E, et al. Notch3 is necessary for blood vessel integrity in the central nervous system. Arteriosclerosis, thrombosis, and vascular biology. 2015; 35:409–20.
57. Roberts AB, Sporn MB. Physiological actions and clinical applications of transforming growth factor-beta (TGF-beta). Growth factors. 1993; 8:1–9. [PubMed: 8448037]
58. Orlova VV, Liu Z, Goumans MJ, ten Dijke P. Controlling angiogenesis by two unique TGF-beta type I receptor signaling pathways. Histology and histopathology. 2011; 26:1219–30. [PubMed: 21751154]
59. Cunha SI, Pietras K. ALK1 as an emerging target for antiangiogenic therapy of cancer. Blood. 2011; 117:6999–7006. [PubMed: 21467543]
60. Larrivee B, Prahst C, Gordon E, del Toro R, Mathivet T, Duarte A, et al. ALK1 signaling inhibits angiogenesis by cooperating with the Notch pathway. Developmental cell. 2012; 22:489–500. [PubMed: 22421041]
61. Gaebel R, Furlani D, Sorg H, Polchow B, Frank J, Bieback K, et al. Cell origin of human mesenchymal stem cells determines a different healing performance in cardiac regeneration. PloS one. 2011; 6:e15652. [PubMed: 21347366]
62. Liu Z, Lebrin F, Maring JA, van den Driesche S, van der Brink S, van Dinther M, et al. ENDOGLIN is dispensable for vasculogenesis, but required for vascular endothelial growth factor-induced angiogenesis. PloS one. 2014; 9:e86273. [PubMed: 24489709]
63. Dombrowski C, Helledie T, Ling L, Grunert M, Canning CA, Jones CM, et al. FGFR1 signaling stimulates proliferation of human mesenchymal stem cells by inhibiting the cyclin-dependent kinase inhibitors p21(Waf1) and p27(Kip1). Stem cells. 2013; 31:2724–36. [PubMed: 23939995]
64. Boulton ME, Cai J, Grant MB. gamma-Secretase: a multifaceted regulator of angiogenesis. Journal of cellular and molecular medicine. 2008; 12:781–95. [PubMed: 18266961]

65. Avery S, Zafarana G, Gokhale PJ, Andrews PW. The role of SMAD4 in human embryonic stem cell self-renewal and stem cell fate. Stem cells. 2010; 28:863–73. [PubMed: 20235236]

66. Rorby E, Hagerstrom MN, Blank U, Karlsson G, Karlsson S. Human hematopoietic stem/progenitor cells overexpressing Smad4 exhibit impaired reconstitution potential in vivo. Blood. 2012; 120:4343–51. [PubMed: 23018642]

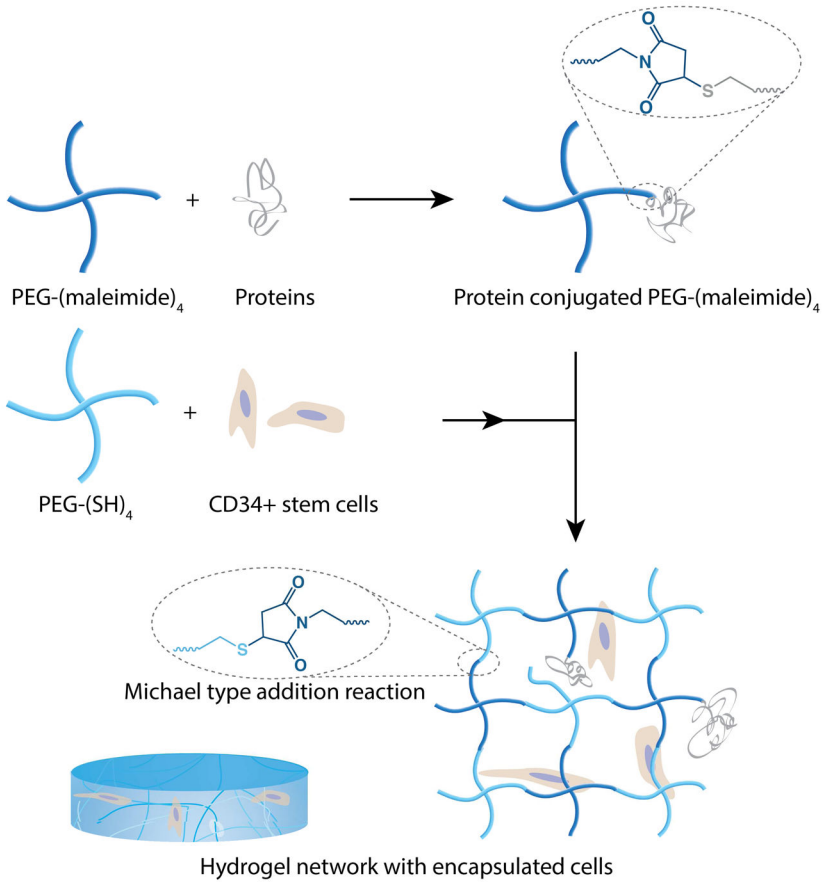

Figure 1. Schematic of hydrogel formation and CD34$^+$ stem cell encapsulation

Synthetic, bioinert PEG hydrogels were prepared by a Michael-type addition reaction between thiol- and maleimide-functionalized four-arm-star PEG. Polymer concentration was varied (3, 4, and 6 weight %) in order to modulate hydrogel stiffness. Cells were suspended in the PEG-thiol solution prior to mixing. Fibronectin (0.0044%) and gelatin (0.032%) were covalently incorporated with the PEG-maleimide prior to hydrogel formation using free cysteine residues. These molecules provided cell adhesion sites within the final material.

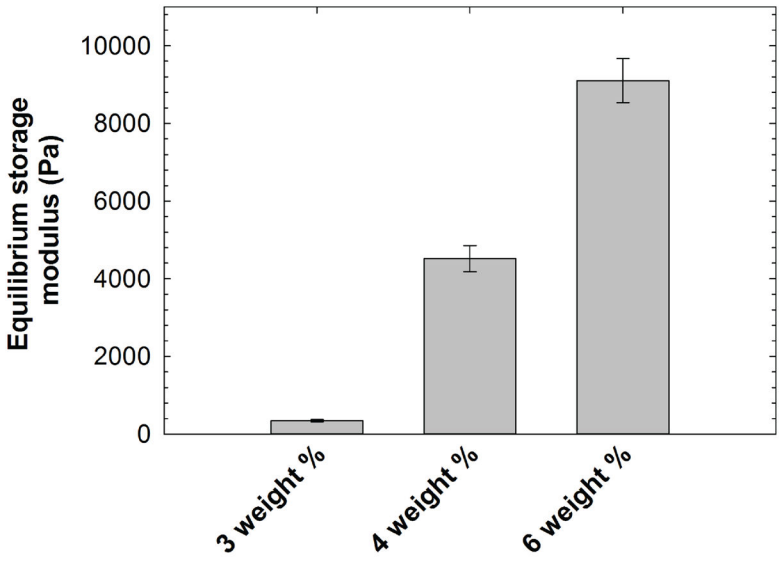

Figure 2. Hydrogel characterization

Equilibrium storage moduli of swollen hydrogels were characterized using oscillatory bulk rheometry. The hydrogels were incubated in StemSpan H3000 medium for 24 hours at 4°C. The swollen modulus of the PEG hydrogels increased with increasing polymer concentration. Gelatin and fibronectin were incorporated during hydrogel formation for introduction of appropriate biochemical cues. The data shown illustrate the mean ($n \geq 4$), with error bars showing the standard error.

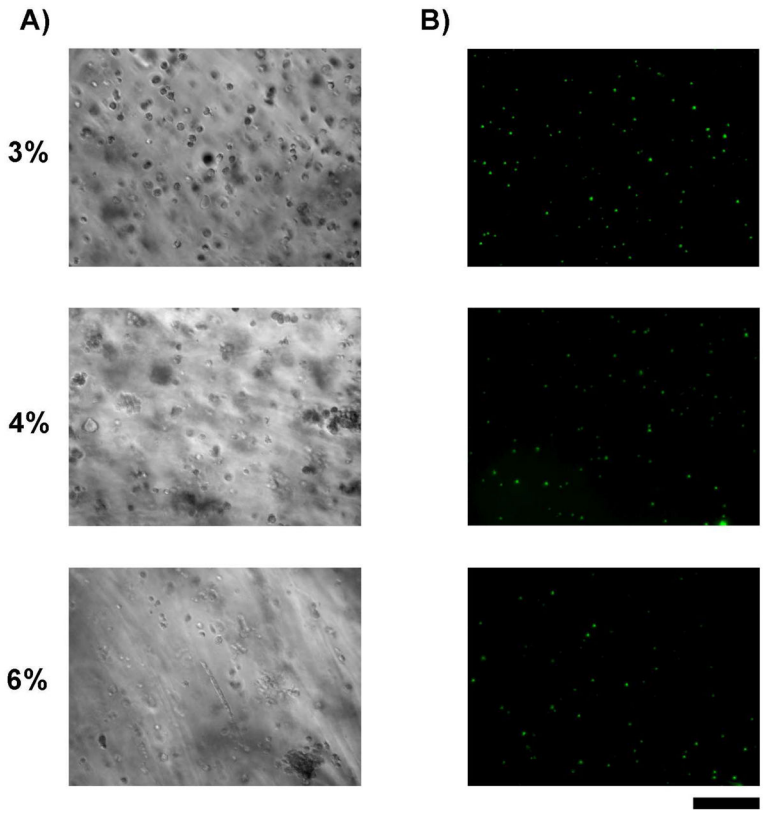

Figure 3. Viability of hydrogel-encapsulated stem cells

A) Cultures of $CD34^+$ cells imaged using Hoffman modulation contrast microscopy. Cells were found singly and in small clusters throughout each gel. **B)** Encapsulated cells within 3, 4, and 6 wt% gels that were grown for 7 days and then stained with cell permeant SYTO13 (green) and cell-impermeant propidium iodide (red) to label live and necrotic cell nuclei, respectively. Cell populations were predominantly SYTO13 positive with virtually no necrotic cells present indicating a high level of cell viability across all gel types. Bar = 200 microns.

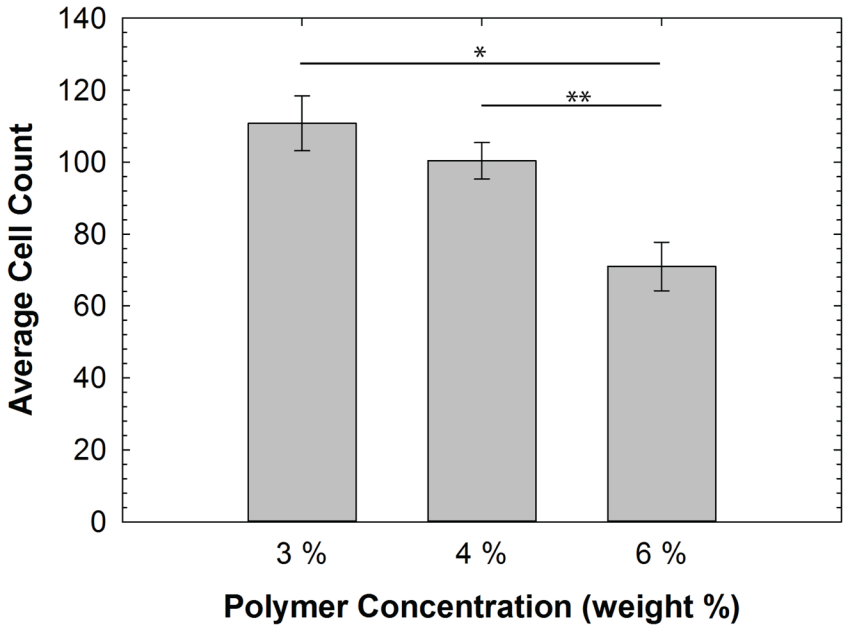

Figure 4. Proliferation of hydrogel-encapsulated stem cells

The average count of cells in hydrogels of each modulus was 110.8 ± 7.6, 100.4 ± 5.0 and 71.0 ± 6.8 (n=5 for each) for 3, 4 and 6 wt% hydrogels, respectively. The proliferation of stem cells was significantly higher in the 3 and 4 wt% gels versus the 6 wt% gels (p=0.005 (*) and p=0.008 (**) respectively by ANOVA with a Tukey's posthoc test).

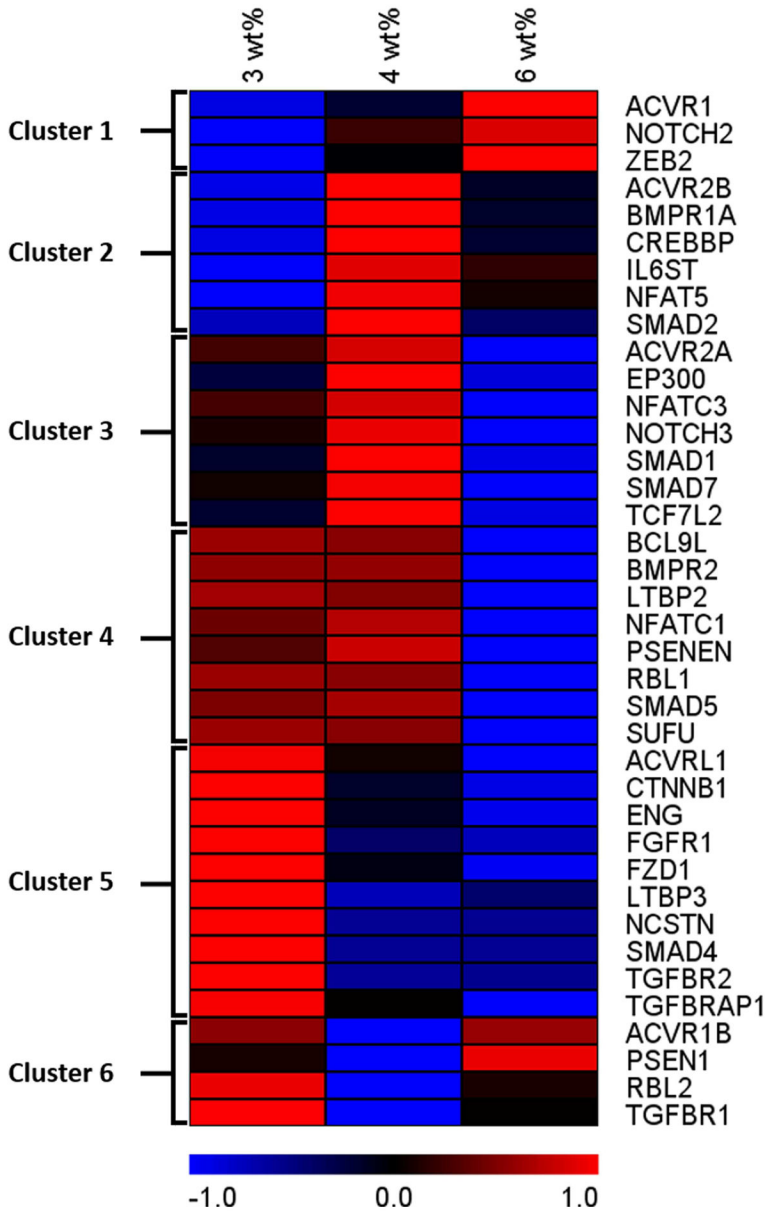

Figure 5. Heat map visualization of gene expression analysis

Heat map generated from the Z-scores (value – mean/S.D.) calculated for RNA microarray results with each gene considered separately. Only targets that were identified as being significantly altered by hydrogel culture were included in the analysis. Expression patterns based on the Z-scores were grouped using a Hierarchical Clustering algorithm (TMEV) and mapped based on a red-black-blue spectrum indicating high to low Z-score. The map shows the patterns of variation in gene expression of stem cells encapsulated in 3, 4 and 6 wt% PEG hydrogels.

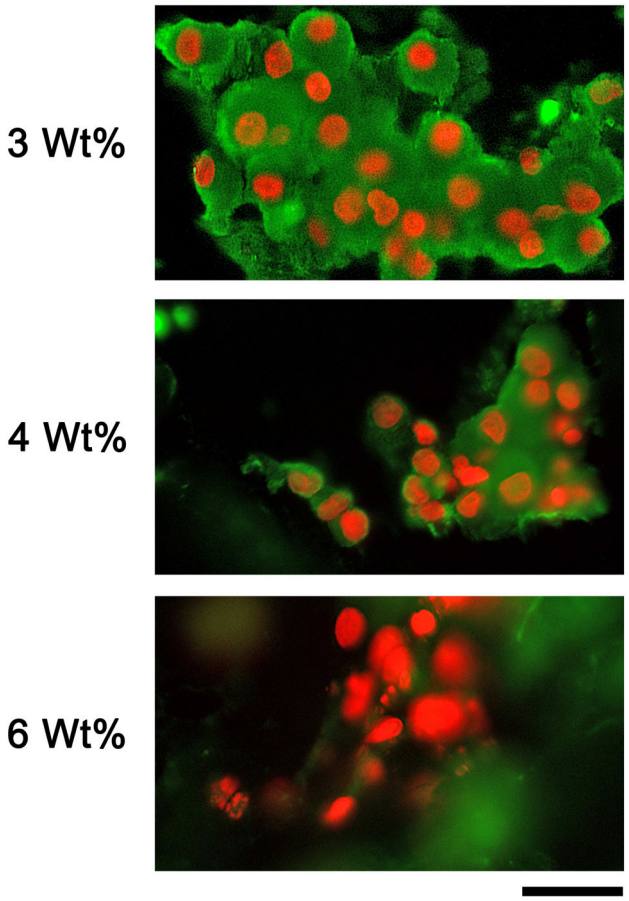

Figure 6. Immunofluorescence detection of endothelial cells in 3D PEG hydrogels

Cells were stained with antibody to von Willebrand Factor to label endothelial cells (pseudo-colored green) and Hoechst 33258 to label nuclei (pseudo-colored red). **A)** Representative cluster of cells from a 3wt% gel culture. Cells stained strongly for vWF and the amount of vWF-positive cytoplasm appeared extensive. Clusters of vWF-positive cells were large, and there were few cells that were vWF negative. **B)** Cells from a 4wt% gel culture. Clusters appeared less extensive, and the amount of vWF-positive cytoplasm appeared to be lower per cell nucleus. **C)** Representative cluster from a 6wt% gel culture. Cells stained weakly or not at all for vWF. Arrows indicate nuclei that appear to be in vWF-negative cells. Bar = 50 microns.

Table 1

Ratio of Hydrogel to TCPS Expression[†]

Symbol	3% (Low)	4% (Medium	6% (High)	Pathway	Cluster
ACVR1	1.114 (0.068)	1.403 (0.005)	2.151 (<0.001)	TGF-β	1
ACVR1B	0.617 (0.003)	0.32 (<0.001)	0.626 (0.003)	TGF-β	6
ACVR2A	1.664 (0.010)	2.502 (<0.001)	0.646 (0.921)	TGF-β	3
ACVR2B	1.239 (0.474)	6.79 (0.002)	2.396 (0.440)	TGF-β	2
ACVRL1	1.284 (0.879)	0.506 (<0.001)	0.159 (<0.001)	TGF-β	5
BMPR1A	0.374 (0.594)	0.714 (0.185)	0.476 (0.408)	TGF-β	2
BMPR2	0.651 (0.598)	0.653 (0.591)	0.466 (0.709)	TGF-β	4
CREBBP	0.38 (0.252)	1.187 (0.028)	0.57 (0.964)	TGF-β	2
ENG	0.909 (0.308)	0.368 (0.008)	0.201 (<0.001)	TGF-β	5
EP300	0.662 (0.007)	0.953 (0.717)	0.560 (<0.001)	TGF-β	3
LTBP2	10.736 (<0.001)	9.856 (<0.001)	3.096 (0.007)	TGF-β	4
LTBP3	2.896 (<0.001)	0.848 (0.021)	1.038 (0.213)	TGF-β	5
RBL1	0.865 (0.049)	0.831 (0.030)	0.261 (<0.001)	TGF-β	4
RBL2	0.732 (0.020)	0.225 (<0.001)	0.447 (<0.001)	TGF-β	6
SMAD1	0.495 (0.551)	1.023 (0.123)	0.322 (0.062)	TGF-β	3
SMAD2	0.871 (0.024)	1.794 (<0.001)	0.997 (0.779)	TGF-β	2
SMAD4	0.598 (0.661)	0.404 (0.046)	0.404 (0.046)	TGF-β	5
SMAD5	0.643 (0.913)	0.678 (0.771)	0.394 (0.111)	TGF-β	4
SMAD7	1.73 (<0.001)	5.528 (<0.001)	0.417 (<0.001)	TGF-β	3
TGFBR1	1.247 (0.032)	0.928 (0.272)	1.079 (0.578)	TGF-β	6
TGFBR2	0.862 (0.020)	0.502 (<0.001)	0.506 (<0.001)	TGF-β	5
TGFBRAP1	0.644 (<0.001)	0.37 (<0.001)	0.203 (<0.001)	TGF-β	5
ZEB2	0.574 (0.028)	0.790 (0.974)	1.111 (0.016)	TGF-β	1
BCL9L	1.364 (0.024)	1.292 (0.051)	0.406 (<0.001)	Wnt	4
CTNNB1	1.098 (0.078)	0.275 (0.265)	0.12 (0.005)	Wnt	5
FZD1	1.638 (0.003)	1.298 (0.039)	1.082 (0.178)	Wnt	5

Symbol	3% (Low)	4% (Medium	6% (High)	Pathway	Cluster
NFAT5	0.730 (0.529)	1.766 (0.003)	1.204 (0.047)	Wnt	2
NFATC1	2.294 (<0.001)	2.643 (<0.001)	1.068 (0.904)	Wnt	4
NFATC3	0.379 (0.819)	0.442 (0.936)	0.26 (0.322)	Wnt	3
TCF7L2	2.451 (<0.001)	2.981 (<0.001)	2.198 (<0.001)	Wnt	3
NCSTN	0.814 (0.016)	0.442 (<0.001)	0.444 (<0.001)	Notch	5
NOTCH2	0.505 (0.984)	1.099 (0.053)	1.593 (0.004)	Notch	1
NOTCH3	5.133 (<0.001)	8.437 (<0.001)	2.532 (0.010)	Notch	3
PSEN1	0.865 (0.612)	0.669 (0.024)	1.043 (0.441)	Notch	6
PSENEN	1.068 (0.378)	1.311 (0.548)	0.578 (<0.001)	Notch	4
FGFR1	10.068 (<0.001)	7.139 (0.003)	6.633 (0.006)	FGF	5
SUFU	0.621 (0.162)	0.585 (0.091)	0.162 (<0.001)	Hedgehog	4
IL6ST	0.787 (0.852)	2.19 (<0.001)	1.524 (0.002)	Pluripotency	2

†Values indicate fold change relative to the TCPS calibrator. p values are given in parenthesis.